Chapter 5

Kinetics of submicron oleic acid aerosols with ozone

Heterogeneous reactions involving particles and gas-phase species can alter important chemical and microphysical properties of aerosols, complicating modeling efforts to assess their effects on climate and human health. Organic aerosols are usually the most abundant component of fine aerosols (< 2 μm) after sulfates, and it is in this size range that one finds those aerosols responsible for the majority of environmental effects[1]. Precursors to organic aerosols include vegetation, the ocean surface, and various combustion processes. Ozone is an important oxidant in the troposphere, often in concentrations sufficient to cause adverse effects on human health and vegetation[2]. Oleic acid is one of a group of organic species proposed as an important tracer species for use in source characterization of ambient aerosols[3]. However, the relative fraction of these species may change as the particle ages, and new product species are likely to be introduced. Very little is known about the kinetics of organic species in atmospheric aerosols. Such knowledge is necessary for quantitative assessment of field studies as well as for use in climate and air quality models often relied upon for regulatory policy decisions intended to safeguard human health.

The relatively recent field of aerosols kinetics has grown out of more general efforts to study gas-liquid interactions. The experimental exploration of such interactions includes approaches involving aerosol levitation devices, Knudsen cells, smog chambers,

horizontal and vertical bubblers, wetted wall or thin film reactors, and droplet trains. Here, we introduce a novel technique for the study of such interactions over a wide range of conditions. For our first set of experiments illustrating the capabilities of the technique, we chose to study the kinetics of oleic acid ($C_{18}H_{34}O_2$) aerosols with ozone. In addition to kinetics information, data from these studies were used to determine the aerosol size change due to uptake of ozone, assess reaction stoichiometry, and obtain qualitative information about the volatility of the reaction products. The size dependence of the aerosol kinetics as discussed by Hanson and Lovejoy is clearly demonstrated[4].

5.1 Experimental approach

The aerosol kinetics apparatus is shown in fig. 5-1. Poly-disperse aerosols, produced in a constant output atomizer (TSI Model 3076) from a solution of oleic acid in methanol, are entrained in a flow of dry filtered air at atmospheric pressure. Most of the methanol evaporates after passing through a silica gel diffusion dryer. (The amount of residual methanol in the particles is estimated from the particle mass spectra to be 2% by weight = 0.15 mole fraction.) The oleic acid aerosols are then carried into a differential mobility analyzer (DMA – TSI Model 3071A). Within the DMA, particles are electrostatically classified by their mobility diameter. Most of the aerosols carry one, two or three charges. Therefore, three or more known sizes are pre-selected and emerge simultaneously from the DMA. The selected distribution can be limited to one, singly charged size by tuning the DMA to large particles (typically > 500 nm in diameter, at the high end of the initial size distribution).

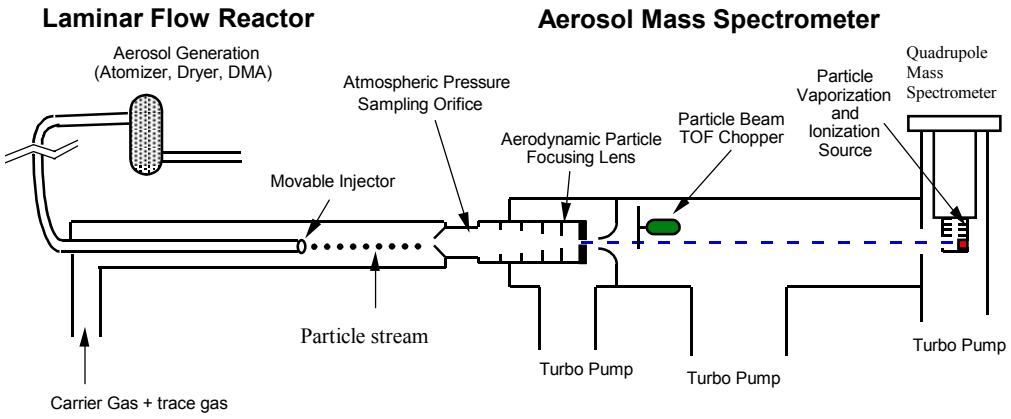

Figure 5-1. The AMS/flowtube apparatus (see fig. 2-1) adapted for aerosol kinetics applications.

The aerosols are then introduced into a 2.2 cm diameter flow tube via a movable injector. Ozone is introduced into the flow tube upstream of the aerosol injector. The flow in the reaction zone is laminar (Re~100) at one atmosphere total pressure. The ozone flows into the flow-tube from behind the exit of the aerosol injector. The relative flow rates in, and radii of the aerosol injector, AMS inlet, and flow-tube are all chosen to optimize conditions for minimizing mixing time between the ozone and the particle stream (~ 1 second) while maximizing the dynamic range of interaction (~10 seconds) under isokinetic flow conditions for the aerosols. Isokinetic (same speed) conditions mean that the aerosol speed (defined by the gas flow speed) does not change upon aerosol delivery or sampling (see appendix). This insures that the particles undergo the least possible changes in drift velocity from the moment they exit the injector into the flow-tube until

they are sampled into the AMS inlet. The isokinetic condition also minimizes mixing in the flow-tube, such that aerosol – trace gas interaction times can be known with high certainty. By matching the flow speeds (~ 8 cm/s) of the carrier gas and injector flows entering the reaction zone, the aerosols are isokinetically injected along the center axis of the flow tube (see appendix).

By translating the injector from 10 to 60 cm, the aerosol-ozone interaction time can be varied from 1 to 7 s. The aerosols are then sampled (again isokinetically) at 1.5 cc/s flow, through a 120 μm orifice opening into the AMS. Isokinetic conditions are necessary for accurate determination of gas-particle interaction times. Due to the low diffusion coefficients of submicron aerosols ($D \sim 10^{-5}$ cm^2/s), there is negligible Brownian diffusion of the aerosols in the absence of convective mixing. This means that the particle stream maintains its initial diameter (defined by the injector diameter, ~ 0.6 cm) over typical measurement times. Once exposed to a known partial pressure of ozone for a known interaction time, the particles are sampled into the AMS inlet for size and compositions analysis.

As described in ch. 2, the AMS consists of three differentially pumped chambers. In the present experiments, velocities range between 150 m/s and 90 m/s for 150 nm and 1 μm particles respectively. The pressures in the next two chambers are 10^{-5} torr and 10^{-7} torr respectively, such that each particle maintains its velocity as it traverses the chambers. In the third chamber the particles strike a resistively heated surface where the aerosols vaporize in 20 to 200 microseconds depending on particle composition and heater temperature. The vapor plume is ionized by electron impact and the resulting ions are mass analyzed with a quadrupole mass spectrometer. It has been experimentally

verified that the mass spectrometer signal at the oleic acid parent peak is directly proportional to the amount of oleic acid in the particles (detection efficiency ~ 10^{-7} ions counted per molecule).

The AMS can be operated in either of two modes: In the TOF mode, signal proportional to the mass of the particles is monitored as a function of TOF or aerodynamic diameter for a given atomic mass unit (AMU). In the mass spectrum mode, the entire mass spectrum of the particles is displayed from 1 to 300 AMU. The TOF signal can be processed in both a single particle mode and in an integrated signal mode. In the integrated mode (used here) the quadrupole current is averaged over 10^3 to 10^4 particles.

By comparing oleic acid particle signal with and without ozone as a function of injector distance for a known ozone pressure in the flow-tube, we are able to plot the fraction of initial oleic acid remaining for different sized aerosols as a function of ozone exposure.

5.2 Results and discussion

In fig. 5-2 we show mass spectra obtained from the vaporized particles of pure oleic acid (solid line) and oleic acid after exposure to ozone (dotted line). In this experimental run the diameter of the particles was approximately 600 nm. The reacted particles were exposed to O_3 at about 10^{-5} atm for 7 seconds. The pure oleic acid mass spectrum in fig. 5-2 compares well with the one in the NIST library[5]. The signal at mass 282 is the oleic acid parent peak. The decrease in this signal in the presence of ozone is clearly evident,

as is the appearance of product peaks at masses 154 and 171. We have chosen the oleic acid parent peak at mass 282 for our kinetic analysis.

The reaction of ozone with oleic acid proceeds most likely via insertion of ozone to the double bond, forming an ozonide with pathways to several possible products[6]. The observed peaks appearing with ozone exposure are likely due to product decomposition at the vaporizing heater or ionizer.

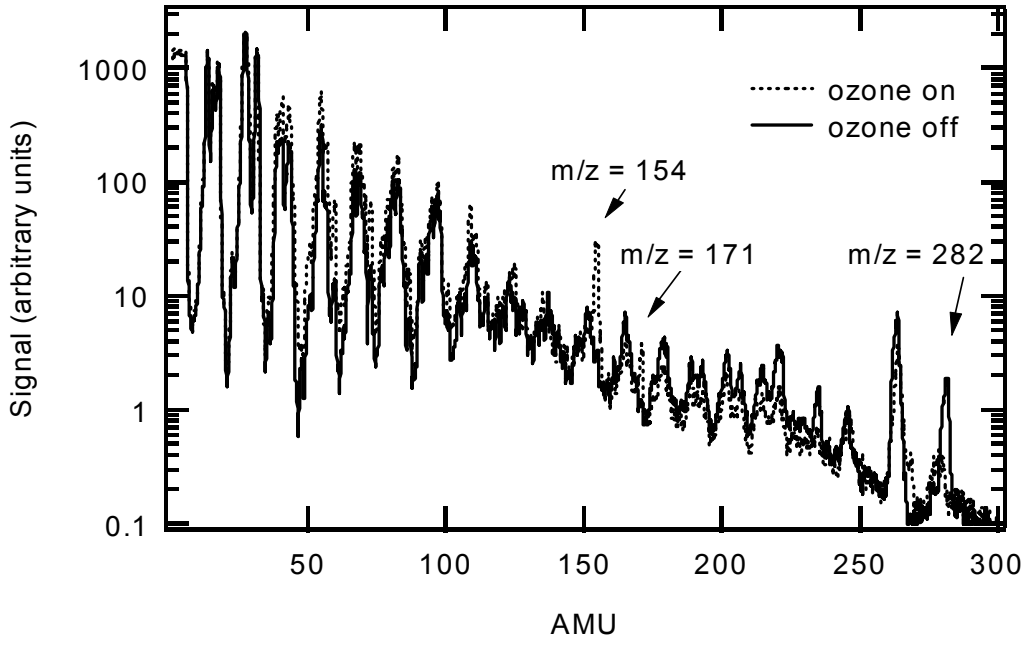

Figure 5-2: Particle mass spectrum for oleic acid aerosols with and without ozone.

The observed mass peaks are consistent with a recent O_3/oleic acid flowtube study of Moise and Rudich[7], who detected heptanoic and azelaic acids in the collected liquid phase.

In fig. 5-3 we show the TOF signals at mass 282 in the absence of ozone and at two ozone exposures ($P_x t$). The top abscissa designates the corresponding aerodynamic diameter of the particles. Three peaks are clearly resolved at 140, 200, and 250 nm corresponding to singly, doubly and triply charged particles. Here, the width of the TOF signals is due mainly to three factors: DMA resolution, which for our flow conditions is

typically $D/\Delta D \sim 15$, chopper transmission period (~0.1 ms), and particle vaporization time[8].

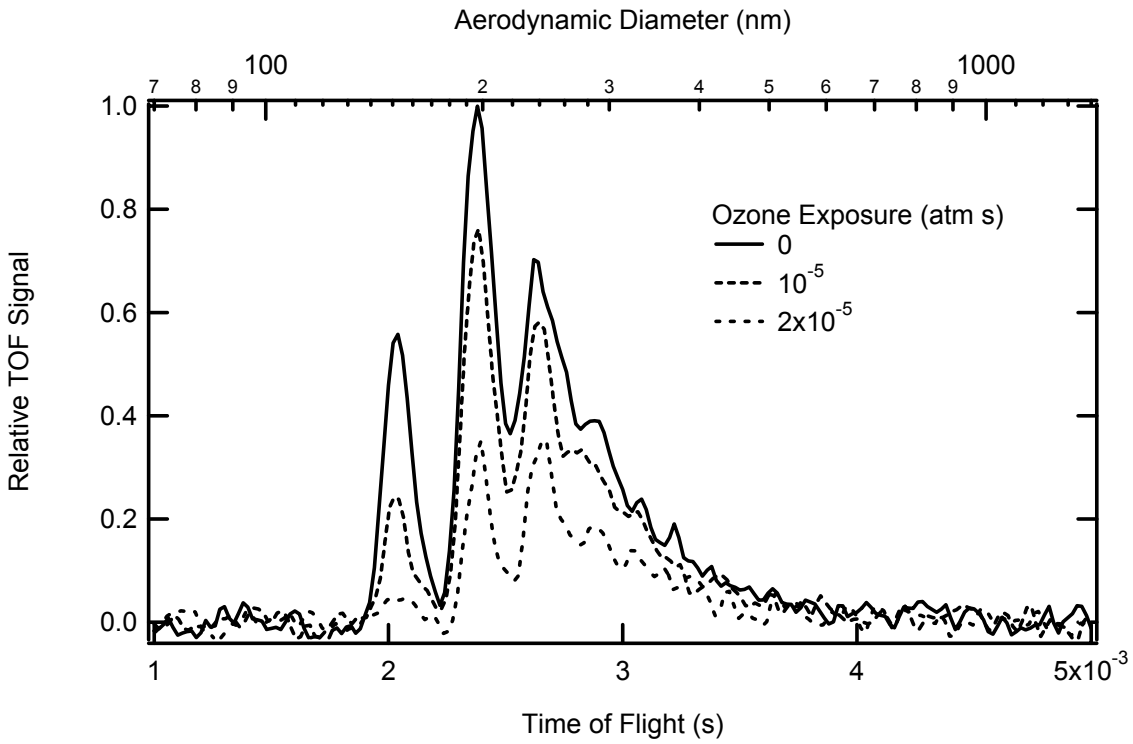

Figure 5-3: Time of flight (TOF) signal (mass 282) for oleic acid aerosol with and without ozone.

Two features are evident in fig. 5-3. The signal at mass 282 decreases significantly with ozone exposure and the fractional loss is greater for smaller diameter particles. For example, at an exposure of 2×10^{-5} atm s, the fraction remaining for the 140 and 200 nm particles is 0.1 and 0.3 respectively.

In fig. 5-4 the TOF signal for 600 nm oleic acid particles (aerodynamic diameter ~ 550 nm) is shown in the absence of ozone and at two exposures. This figure highlights

two other features present in the TOF data: a) An increase in particle size with ozone exposure is evident in the rightward shift in the leading edge of the TOF signal. This shift is simultaneous with the decrease in oleic acid signal due to species reaction. For the $4x10^{-5}$ atm s ozone exposure, the observed increase in time of flight is 25 μs which for the 600 nm oleic acid particles corresponds to a fractional volume increase of $\Delta V/V_0$ = 0.06 (D/D_0 = 1.02). b) Also in fig. 5-4, it is apparent that the signal width is decreasing with reaction extent. The full width at half max is 0.34, 0.24, and 0.18 ms for 1.0, 0.4, and 0.2 fraction remaining respectively. We suggest that the decrease in the TOF width is due to faster vaporization of the particle as it strikes the vaporizing heater. This decrease is consistent with increased volatility of the reaction products compared to unreacted oleic acid.

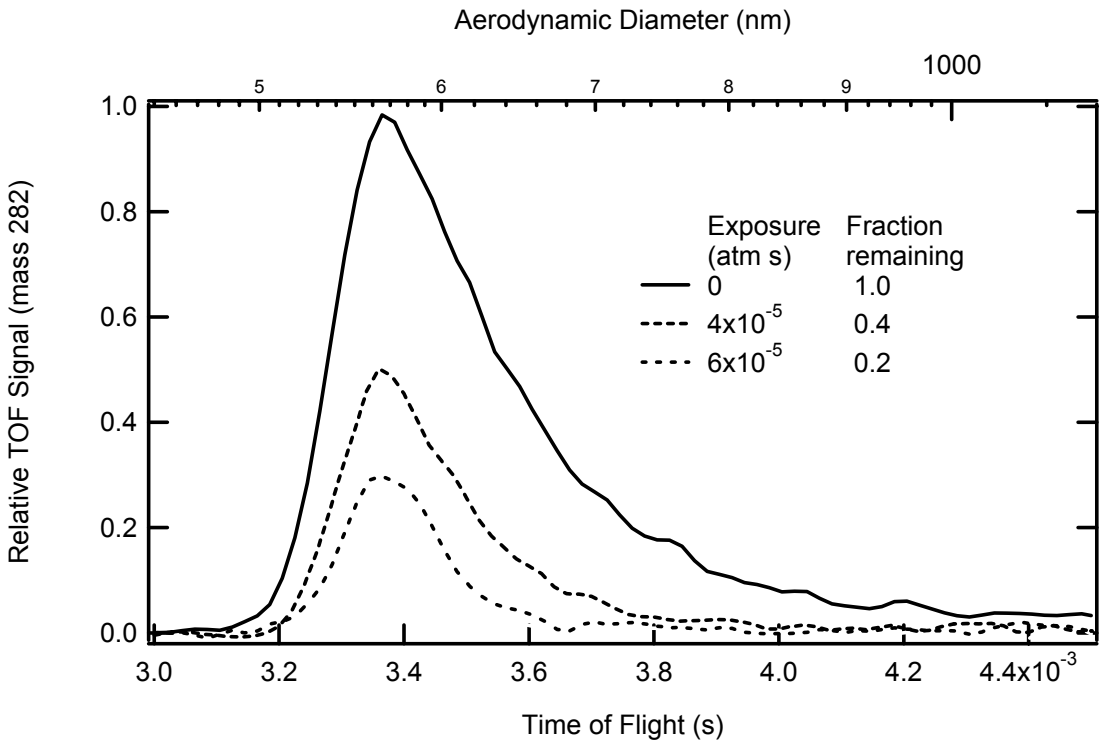

Figure 5-4: TOF signal (mass 282) for 600 nm diameter oleic acid aerosol without ozone and at two ozone exposures.

The data shown in fig. 5-2 can be quantitatively analyzed to provide information about the stoichiometry of the reaction. The integrated ion signal of the mass spectrum from 0 to 300 amu is proportional to the total aerosol mass (assuming detection efficiency is mass independent over the range of interest). Fig. 5-5 plots the ratio of this total mass for ozone-on to ozone-off signals as a function of fraction oleic acid reacted, obtained from the signal ratios at the parent mass (282). The data points fall within ~5% of the solid line which is the expected integrated mass ratio if a single O_3 molecule reacted with each oleic acid molecule, and the products were retained in the particle. Under such

assumptions, the ratio of the new to old mass as a function of reaction extent, ε or fraction reacted (1-fraction remaining) is:

$$\frac{m}{m_0} = 1 + \frac{nM_x}{M_y}\varepsilon \tag{5.3}$$

Here n is the number of ozone molecules reacting per oleic and M_x and M_y are the molecular weights of ozone and oleic respectively. The dashed line assumes that two ozone molecules react per oleic acid molecule (n = 2). As is evident, the former is consistent with the results. Similar information is obtained from the data in fig. 5-4 by converting the change in TOF (measuring particle diameter) to a mass change (see below).

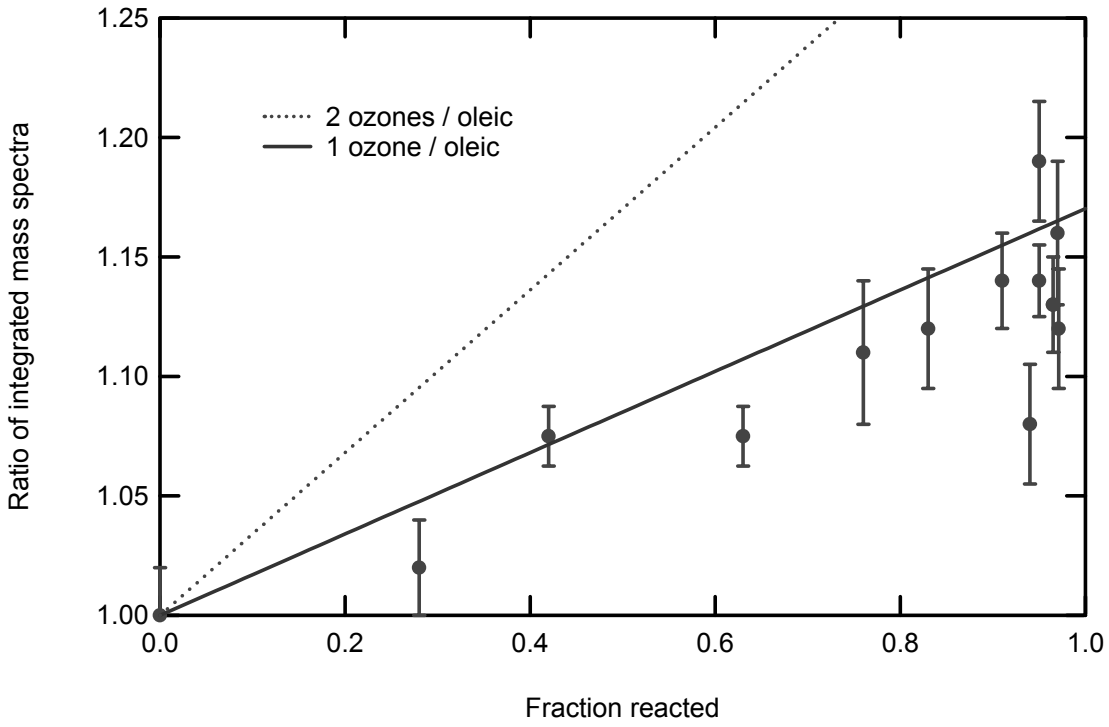

Figure 5-5: Ratio of the integrated mass spectra as a function of fraction reacted.

5.3 Kinetic modeling

Gas-phase uptake experiments are typically complicated by efforts to correct for gas-phase diffusion. In our experiments, the characteristic time for gas-phase diffusion is less than 10^{-5} s. On the other hand, the characteristic time for reaction within a thin shell (see ch. 4) of the aerosol is on the order of 1 s, so no gas phase diffusion correction is necessary (see plot, fig. 4-4). Furthermore, this is the largest characteristic time such that a model evoking oleic reacting in a thin shell is the most appropriate. In such a model, ozone attains its Henry's law equilibrium value immediately at the surface. Very quickly thereafter a pseudo-steady state concentration profile of ozone is established within the

aerosol. It is important to note that such a profile depends on the concentration of organic within the particle; the ozone will diffuse more deeply on average into the particle the less organic there is for it to react with. A further simplifying assumption is that there be no oleic concentration gradient within the particle. This is justified by the very short characteristic time for oleic diffusion to the surface (~10^{-4} seconds). Diffusion of oleic into any potentially depleted region would be much faster than the rate of reaction there, such that no appreciable gradient in oleic concentration would be allowed to form.

The reactive uptake coefficient is therefore expected to govern the overall rate. A key parameter in the formulation of Γ_{rxn} is the ratio l/a, where a is the particle radius and l is the reacto-diffusive length, given by $l = (D/k_2[Y])^{1/2}$. Here D is the diffusion coefficient ($cm^2\ s^{-1}$) of ozone in oleic acid, k_2 is the second order rate constant for the reaction between ozone and oleic acid, and $[Y]$ is the concentration of oleic acid.

The magnitude of l can be estimated as follows. The initial concentration, $[Y]_0$ is 3.15 M. The parameters D and k_2 have not been measured, however, they are expected[9] to be on the order $D \sim 10^{-6}$ $cm^2\ s^{-1}$ and $k_2 \sim 10^6$ $M^{-1}\ s^{-1}$. With these values, the reacto-diffusive length is estimated to be $l \sim 5$ nm. This is less than 10% of the radius for even the smallest particles studied here. In this limit, Γ_{rxn} is (see sec. 4.3.3 above):

$$\Gamma_{rxn} = \frac{4HRT}{\bar{c}}\sqrt{Dk_2[Y]} \qquad (5.4)$$

Here, H (M atm^{-1}) is the Henry's law coefficient for ozone in oleic acid, R is the gas constant (8.206×10^{-2} atm K^{-1} M^{-1}), T is the temperature, and $\bar{c}$ is the mean thermal speed of the impinging trace gas (cm s^{-1}). The experimentally monitored quantity is the fraction of initial particle species $[Y]/[Y]_0$ remaining after a given exposure time at a known

ozone pressure. With Γ_{rxn} given by eq. 5.4, this fraction can be expressed (see eq. 4.34 above) as,

$$\sqrt{\frac{[Y]}{[Y]_0}} = 1 - \frac{3\,H\,\sqrt{Dk_2}}{2\,a\,\sqrt{[Y]_0}}\,P_x t \qquad (5.5)$$

where, P_x, is the partial pressure of ozone (atm). In eq. 5.5 we have assumed a (cm) to be constant during the uptake process. Here the exposure, $P_x t$, is the experimental variable. This expression indicates that the fractional consumption of oleic acid is more rapid in smaller particles, as is observed experimentally (fig. 5-3). Further, the model predicts that a plot of $([Y]/[Y]_0)^{1/2}$ as a function of the exposure yields straight lines with slopes inversely proportional to the particle radius.

We note that as the 0.6 cm diameter particle stream enters the reaction zone, the particles do not immediately come into contact with the reactant trace gas (in this case O_3). The trace gas must mix with the particle stream. If we assume that during some effective mixing time τ, the aerosols are not in contact with the reactive gas, then the effective reaction time is $(t - \tau)$, which is to be substituted in eq. 5.5.

In fig. 5-6 we show plots of $([Y]/[Y]_0)^{1/2}$ as a function of $P_x(t-\tau)$ for three particle diameters; 200 nm, 400 nm, and 600 nm. The straight lines in the figure show the global fit to the experimental data with two fitting parameters; $H(Dk_2)^{1/2}$ and τ. With a and $[Y]_0$ given ($[Y]_0 = 3.15$ M), best fit to the data is obtained with $H(Dk_2)^{1/2} = 0.33 \pm 0.03$ ($M^{1/2}$ atm cm s^{-1}) and $\tau = 0.35$ s. The effective mixing time of 0.35 s is consistent with the characteristic diffusion time into a 0.6 cm diameter stream (~ 0.5 s). We note that the same value of the product $H(Dk)^{1/2}$ fits the kinetics of the reaction over the full range of oleic acid decay. In the face of this result, one is led to conclude that the parameters *H,*

D, and *k* either remain the same from reactant to product, or are changing in opposing directions such that the product remains nearly constant.

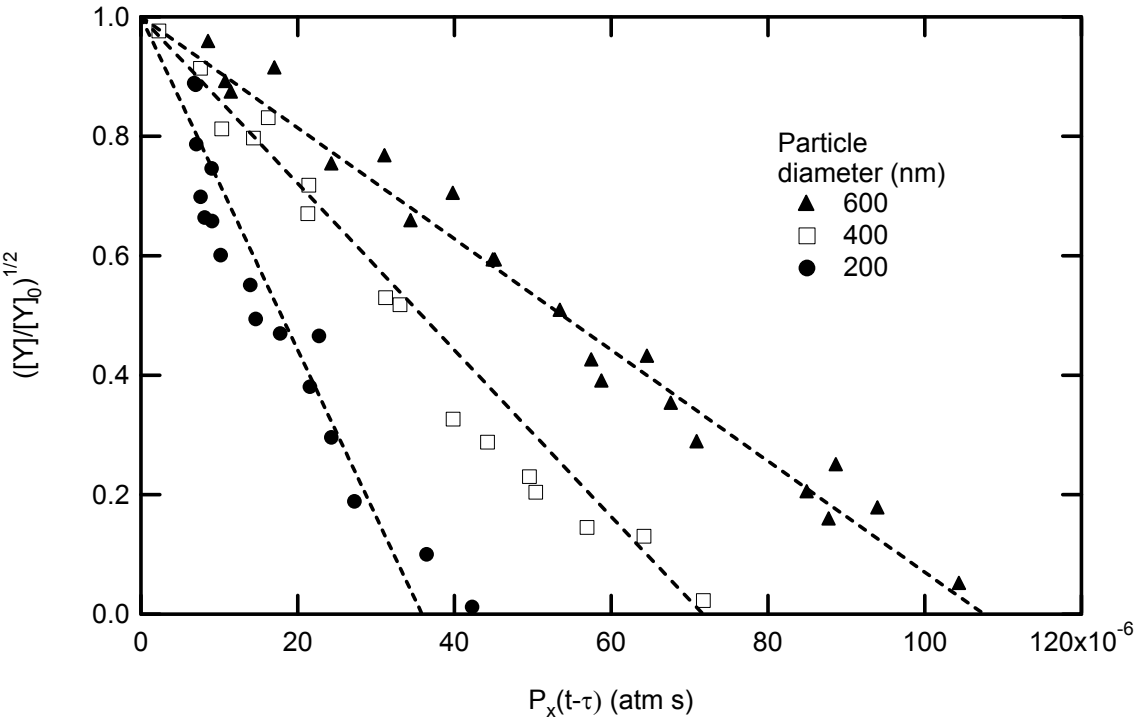

Figure 5-6: Oleic acid depletion in the form $([Y]/[Y]_o)^{1/2}$ as a function of exposure $P(t-\tau)$ for aerosol diameters 200, 400 and 600 nm. The dashed lines are model fits to the data.

As is evident, the observed oleic acid decay is in accord with the model, clearly exhibiting size dependent aerosol kinetics. With the fitted value of $H(Dk_2)^{1/2}$, eq. 5.4 yields the reactive uptake coefficient for ozone on oleic acid, $\Gamma_{rxn} = 1.6\ (\pm 0.2) \times 10^{-3}$, in reasonable agreement with wetted wall experiments performed by Moise and Rudich

using O_3 and oleic acid and by de Gouw and Lovejoy [10] using O_3 and other liquid alkenes.

In choosing the model to describe the present experiments we assumed that the reacto-diffusive length was much smaller than the particle radius ($l<<a$). Using the more general formulation of the reactive process (allowing $l \sim a$) as in eq. 4.19, the model is observed to fit the data only for $l < 10$ nm. This defines an upper limit on the value $l=(D/k_2[Y]_0)^{1/2}$. With $[Y]_o$ known, it follows that $D/k_2 < 3.2 \times 10^{-12}$ cm^2 M. An order of magnitude value for H of ozone in oleic acid is estimated to be 10^{-1} M atm^{-1}, using earlier approximated values for D and k_2.

We also performed experiments as a function of relative humidity and could detect no change in the rate of chemical processing within the oleic acid particles from 3% to 80% relative humidity.

5.4 Atmospheric implications

The value of $H(Dk_2)^{1/2}$ obtained from data analysis implies an atmospheric half-life with respect to O_3 reaction on the order of minutes for submicron aerosols of pure oleic acid in atmospheres polluted with 100 ppb O_3. On the other hand, in the Los Angeles area, field measurements together with source flux estimates, imply an oleic acid atmospheric lifetime on the order of days[11]. The longer atmospheric lifetime is likely due to the fact that oleic acid in atmospheric aerosols can be found in semi-solid, highly viscous mixtures such as with stearic and palmitic acids present[12]. Diffusion coefficients for gases in solids are typically 10^5 times smaller than in liquids so trapping the oleic acid in a solid matrix would diffusively shield it from the incoming ozone, leading to a much longer

lifetime. Indeed, the quantitative nature of our result enables us to extrapolate to approximate "solid" oleic acid lifetimes by virtue of the expected changes on $H(Dk)^{1/2}$. The diffusion coefficient, D for O_3 in solids is expected to be 10^5 times smaller, such that $H(Dk)^{1/2}$ will be almost 10^3 times smaller, and the lifetime passes from minutes to days, consistent with field observations. Also, the existence of a short reacto-diffusive length (l < 10 nm) would confine the reaction to a thin shell near the surface of the aerosol, so that in such viscous particles the reaction is slowed down by diffusive transport of oleic acid to the surface (see sec. 4.2.4 above). Another possibility is the existence of a thin ammonium nitrate shell encapsulating the organic aerosol, which would be solid at low relative humidity[13].

5.5 Directions for future research

This section is designed to benefit the researcher using aerosol mass spectrometry with thermal vaporization schemes such as the AMS used here. The treatment is commentary in nature, purposing to outline future research directions. In many cases, these experiments were attempted, and potential pitfalls are summarized where applicable.

Elaidic acid is an especially interesting follow-up to oleic acid from the standpoint of particle morphology. Elaidic acid has very similar chemical structure to oleic acid (same location of double bond, same molecular weight), but it is a solid at room temperature. Such experiments would help elucidate the role of particle phase in aerosol kinetics, and could progress to mixtures of oleic and elaidic acids in such a way as to develop a model of phase/size dependent kinetics. Preliminary efforts to measure the kinetics of elaidic acid and ozone showed no difference from the oleic/ozone system. We

concluded that leftover solvent within the elaidic particles made them liquid while reacting with ozone in the flowtube.

Another mixture of interest is oleic and stearic acid. Stearic acid is identical to oleic except that it has no double bond, and is a solid at room temperature. Initial experiments performed on this system yielded no discernible difference in rate when compared to the pure oleic particles. As was previously noted, particles generated in the atomizer are typically not completely devoid of solvent. This may be even more important for solid particles whose exteriors may dry first, encapsulating the remaining solution within the particle.

Nucleation/condensation particle generation

One possible technique for drying particles produced from the atomizer would be to heat them while flowing them through a drying tube. This may lead to complications however as some organics decompose upon heating. Mixtures of atmospherically relevant organic and inorganic species can perhaps best be made mimicking actual production processes in the atmosphere. An example would be to evaporate mixtures of organics and then re-condense them within a cooled flow of gas, either on a seed aerosol or through homogeneous nucleation. Such particle generators have been developed, including the Sinclair-LaMer model. Such condensation particle generation typically produces very homogeneous (single size) aerosol ensembles, easily controlled by adjusting flow conditions and heating temperatures (vapor pressure of species to be condensed).

Information from particle size change

In the case of reactive uptake of trace gas, particles in general undergo both mass and density changes. As mentioned above, there was some detection of size change with

reaction in the case of oleic acid and ozone, although evidence of density change complicated analysis such that quantitative conclusions could not be drawn. Changes in the aerodynamic diameter of the particle can be expressed as:

$$\frac{D_a}{D^o{}_a} = \left(\frac{s(\varepsilon)}{s^o}\right)^{2/3}\left(1 + \frac{nM_x}{M_y}\varepsilon\right)^{1/3} \tag{5.6}$$

Here $D^o{}_a$ and D_a are the aerodynamic diameters of the particle before and after reaction, s is the specific gravity of the particle, and ε is the reaction extent. This expression follows from conservation of mass (eq. 5.3) and the definition of the aerodynamic diameter for spherical particles ($D_a = sD$). The "mass" term on the far right increases with reaction extent ε, while if there is a decrease in specific gravity, s with reaction, the first term decreases with stronger functional dependence. Another way of looking at eq. 5.6, is that for a known reaction extent, we can calculate the specific gravity from the ratio of aerodynamic diameters.

Chapter 5 Appendix

Deriving conditions for isokinetic sampling in laminar flow studies

In this appendix we develop expressions for isokinetic sampling conditions to be used in aerosol kinetics (as in ch. 5) or microphysics (as in ch. 6) studies. For kinetics studies, this condition enables accurate calculation of aerosol – reactive trace gas interaction time. In microphysics studies, this condition insures that a size distribution is not biased upon sampling into an inlet for detection, as with an AMS.

Poiseuille's law[14] gives the speed, u of an air stream under laminar flow conditions a distance r from the center of a cylindrical tube of radius R and length L:

$$u(r) = \frac{1}{4\eta}\frac{\Delta p}{L}(R^2 - r^2) \tag{A5.1}$$

Here Δp is the pressure difference driving the flow and η is the viscosity of air. The velocity at the walls is zero here, to satisfy the no-slip boundary condition. To link the constants with a more experimentally relevant quantity, we integrate to link the constants with the total volume flow rate:

$$Q = \int_0^R u(r)2\pi r dr = \frac{\pi}{8\eta}\frac{\Delta p}{L}R^4 \tag{A5.2}$$

Now we can use the same approach to write an expression for the volume flow rate through the radial domain (defined by the injector cross section – see fig. A5-1) extending from $r = 0$ to $r = r_{inj}$:

$$Q_{inj} = \int_0^{r_{inj}} u(r)2\pi r dr = \frac{2Q}{R^4}(R^2 {r_{inj}}^2 - \frac{{r_{inj}}^4}{2}) \tag{A5.3}$$

Here, we have used eq. A5.2 to express Q_{inj} as a function of Q. This is the flow rate through a radial domain of the flowtube with the same cross section as the injector (see fig. A5-1). The average velocity within this cross section is given by $Q_{inj}/\pi r^2_{inj}$. This is of course identical to the average velocity within the injector itself, by definition. It follows that setting Q_{inj} to the value given by eq. A5.3 assures that the average speed of the particles leaving the injector will be equal to the average speed of the air in the flowtube over the domain of the injector. The choice of injector flowrate is thus constrained by the choice of flowtube flow rate, Q and radius, R. Once the particles have been entrained within the flowtube, they are sampled into the AMS inlet (see fig. A5-1). We can extend the same arguments to establish isokinetic conditions at the inlet to the AMS. Having established an analogous expression to A5.3 for the inlet, we may divide the two and obtain:

$$\frac{Q_{inj}}{Q_{inl}} = \frac{R^2 {r_{inj}}^2 - {r_{inj}}^4/2}{R^2 {r_{inl}}^2 - {r_{inl}}^4/2} = \frac{{r_{inj}}^2 (R^2 - {r_{inj}}^2/2)}{{r_{inl}}^2 (R^2 - {r_{inl}}^4/2)} \qquad \text{(A5.4)}$$

In the limit where $r_{inj} << R$ and $r_{inl} << R$ this gives the same result as if we were to simply match the average velocities of the injector and the inlet. In fact, a reasonable approximation to the condition met by eq. A5.4 is to set each average velocity equal to the maximum within the flowtube, or twice the average.

Under such conditions the drift velocity of the aerosols sampled at the inlet is given by:

$$v_{drift} = \frac{2Q}{\pi R^4}\left(R^2 - \frac{{r_{inl}}^2}{2}\right) \qquad \text{(A5.5)}$$

Eq. A5.5 represents the laminar flow velocity field averaged over the radial domain (cross section) defined by the AMS inlet, and it is an accurate aerosol drift velocity in the limit of no convective or Brownian aerosol mixing.

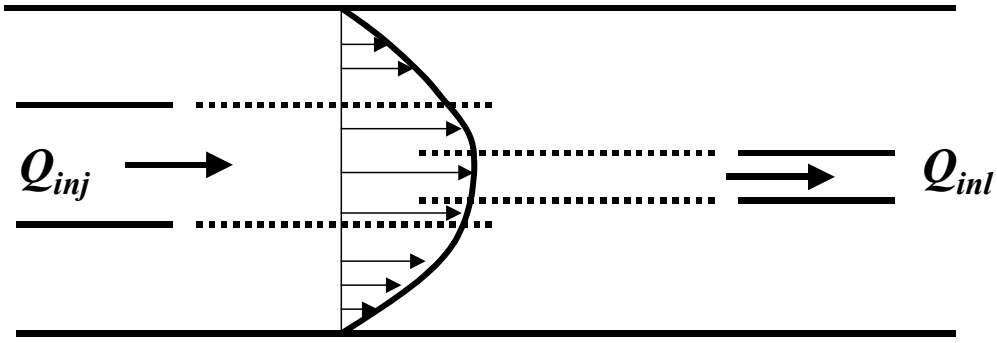

Figure A5-1: Isokinetic delivery and sampling in laminar flow requires matching flow velocities over radially averaged domains at both the injector and inlet.

Typically the injector flowrate will be fixed. Since flowtube, injector and inlet geometries will fix other flows according to eq. A5.4, one must choose the geometry most appropriate for the study. In general, one desires short mixing times for reactive trace species into the particle stream and long trace gas/ particle interaction time. The characteristic time for flow into a particle stream of radius r is $r^2/\pi^2 D$ (D is the trace gas diffusion coefficient), whereas interaction time is inversely proportional to Q (fixed by Q_{inl} if isokinetic). The geometry must therefore be optimized for the system of interest. In the system yielding results presented here, a minimum Q_{inj} was required to get sufficient particle signal. This defined the minimum r_{inj} thus defining the operational geometry and flow for these studies.

Chapter 5 References

[1] M. C. Jacobson, H. Hanson, K. Noone, and R. Charlson, *Reviews of Geophysics*, **38**, 267 (2000).

[2] J. Seinfeld and S. Pandis, *Atmospheric Chemistry and Physics*, (John Wiley & Sons, 1998, 107).

[3] J. J. Schauer, W. F. Rogge, L. M. Hildemann, M. A. Mazurek, G. R. Cass, and B. R. Simoneit, *Atmos. Env*, **30**, 3837 (1996).

[4] D. R. Hanson and E. R. Lovejoy, *Science*, **267**, 1326 (1995).

[5] NIST/EPA/NIH Mass Spectral Library, Search / Analysis Programs and Data for Microsoft Windows 95, 98, NT, 2000, January 2001.

[6] S. Rakovsky and G. Zaikov, *Kinetics of Ozone Reactions with Organic and Polymeric Compounds in Liquid Phase* (Nova Science Publishers, 1998, 112).

[7] T. Moise and Y. Rudich, submitted to *J. Phys. Chem.,* 2002.

[8] J. Jayne, D. Leard, Z. Zhang, P. Davidovits, C. Kolb, and D. Worsnop. *Aerosol Sci. Technol*.**, 33**, 49 (2000).

[9] Rakovsky, et al., p. 125.

[10] J. A. de Gouw and E. R. Lovejoy, *Geophys. Res. Lett.,* **25**, 931 (1998).

[11] W. F. Rogge, L. M. Hildemann, M. A. Mazurek, G. R. Cass, and B. R. T. Simoneit, *Environ. Sci. Technol*., **25**, 1112 (1991).

[12] J. J. Schauer, M. J. Kleeman, G. R. Cass, and B. R. T. Simoneit, *Environ. Sci. Technol*., **33**, 1566 (1999).

[13] A. S. Wexler and J. H. Seinfeld, *Atmos. Env*., **24A**, 1231 (1990).

[14] T. E. Faber, *Fluid dynamics for physicists*, (Cambridge, 1995).